Magnetic Surfaces of the W VII A Stellarator

H.J.Jäckel, J.Kißlinger, F.Rau

IPP 2/231 August 1976

MAX-PLANCK-INSTITUT FÜR PLASMAPHYSIK

8046 GARCHING BEI MÜNCHEN

MAX-PLANCK-INSTITUT FÜR PLASMAPHYSIK

GARCHING BEI MÜNCHEN

Magnetic Surfaces of the W VII A Stellarator

H.J.Jäckel, J.Kißlinger, F.Rau

IPP 2/231 August 1976

Die nachstehende Arbeit wurde im Rahmen des Vertrages zwischen dem Max-Planck-Institut für Plasmaphysik und der Europäischen Atomgemeinschaft über die Zusammenarbeit auf dem Gebiete der Plasmaphysik durchgeführt.

IPP 2/231

H.J.Jäckel
J.Kißlinger
F.Rau

Magnetic Surfaces of the
W VII A Stellarator.
August 1976 (in English)

ABSTRACT

Properties of the magnetic field of the Garching stellarator WENDELSTEIN VII A are studied experimentally, using a pulsed electron beam at reduced magnetic fields. Nested magnetic surfaces are shown to exist within the limiter radius, for values of the rotational transform $\iota \leq 1/4$. Up to $\iota = 0.72$ the shape of the experimental magnetic surfaces is nearly identical to that of computed surfaces, and computed values of ι agree within a few % with the experiment. As expected for a $\ell = 2$ stellarator, the shear is small; $d\iota/dr > 0$. Analytic approximations are derived for various relationships between the currents in the field systems, the rotational transform and the radial coordinate. Stray radial and vertical fields present in the installation are inferred from experiments without helix current and from the observed shift of the magnetic axis. They appear to be mainly proportional to, and amounting to about 0.4 % of, the toroidal field. For irrational $\iota \approx 0.23$, an applied local and predominantly radial field of up to 2 % of the toroidal field shifts the magnetic axis and changes ι, but does not destroy the configuration. For rational $\iota = 1/4$, magnetic islands could not be identified experimentally. They are calculated to exist with a radial dimension of about 20 % of the limiter radius, caused by certain construction elements of the helix conductors. An increased shear, which would be produced by a torsatron configuration in W VII A, would reduce the size of these islands.

INTRODUCTION

The magnetic field of the Garching stellarator WENDELSTEIN VII A is investigated using a pulsed electron beam at low magnetic fields in order to study properties of the stellarator field of this particular device "in situ", thus supporting numerical field calculations by direct experimental evidence. Special interest in the present investigation is directed in

- proving the existence and radial extension of magnetic surfaces,
- establishing the range of useful variation of the rotational transform,
- obtaining evidence of magnitude and scaling of stray fields, and
- contributing to the question of magnetic island formation at rotational values close to rational numbers.

The design and technical details of the W VII A stellarator are described elsewhere |1|. Data relevant for this paper are summarized in Table I. The magnetic configuration produced by identical currents in the helix and the toroidal field system will be referred as the standard case configuration in this paper.

The following systematics of the W VII A field configuration are valid: At the azimuth of the experimental ports the long sides of the approximately elliptic magnetic surfaces are inclined by $\pm$ 45° with respect to the radial direction, the orientation changing its sign between successive port planes. Since the polarity of the helix currents was not changed during the course of the present investigation, the

long side of the magnetic surface lies between the radial and the upper vertical port for an odd number p of the experimental ports situated at an azimuthal position $\varphi = p \cdot 36^{\circ}$ and a toroidal field directed parallel to the azimuthal coordinate[+)], or for an even port number at a toroidal field being antiparallel to φ.

A vertical field pointing downward shifts the magnetic axis radially outward, and a radial field directed outward introduces an upward offset of the magnetic axis, if the toroidal field is parallel to φ. Changing the polarity of one of these fields changes the direction of this offset of the magnetic axis.

EXPERIMENTAL METHOD AND STANDARD CASE OF W VII A FIELD CONFIGURATION

The experimental method is simple: A pulsed electron beam (current up to 10 μA, energy 25 eV, pulse length 4 μs equivalent to a beam length of $L \approx 2 \pi R_o \approx 12$ m, repetition rate about 300 Hz) is provided by an electron source adjustable parallel to the magnetic field. Electrostatic deflection plates allow an ExB-shift of the electron beam off the source. This avoids absorption of the beam by the source after one or more transits in the poloidal direction. The electron beam is localized by a small shielded probe. The electron source and the probe are mounted at azimuthal angles $7 \cdot 36^{\circ}$ and $5 \cdot 36^{\circ}$, respectively, the limiter being placed at $\varphi = 0$. In their observation planes, the positions of the electron source and the probe are known within 1 - 2 mm. The beam is monitored by a capacitively coupled plate. The signal of this monitor changes when the beam interacts with the probe shaft, thus aiding to localize the beam by the probe. Phase-focussing of the electron beam as described in Ref./2/ is not used. In a pilot experiment it was found to be effective and increased the probe signal of certain transits by about a factor of three. Although possibly the conditions were not yet optimized, this improvement was considered not to be essential.

+) Called polarity "A" of the toroidal field current.

The magnetic field confines the beam within a transverse dimension of about 1 mm. Electrostatic forces of the electrons tend to spread the beam in time. This decreases the amplitude of the probe signal, in addition to the interaction of the beam electrons with the rest gas in the torus.

The number N of transits the long way around the torus is obtained from the time difference between the start pulse applied to the source and the maximum of the probe signal. At good vacuum conditions ($p_o \approx 3 \cdot 10^{-7}$ torr in the torus) up to 450 transits are obtained, equivalent to a total length of the field line of about 6 km.

In a stellarator field having closed magnetic surfaces, charged particles follow drift surfaces [2] which deviate periodically from the magnetic surfaces. These deviations are of the order of ϱ/t, ϱ being the Larmor radius, unless the helical mirrors of the stellarator and/or the perpendicular velocity of the particles are excessive [3,4]. In the present investigation ϱ/t is kept below 1 mm in most of the experiments. Here we assume that 1 % of the energy of the beam is transverse to the magnetic field. Consequently, the deviation between drift surfaces and magnetic surfaces can be neglected, as was shown both experimentally and also by computation of drift surfaces [5]. In experiments performed at low toroidal field, the electron beam is directed both parallel and antiparallel to the toroidal field, and the resulting surfaces are averaged.

A nest of experimental magnetic surfaces is shown in the upper half of Fig. 1. The toroidal field coils and the helix carry identical currents. This ensures high temporal stability of the magnetic topology and a rotational transform constant in time.

The experimental procedure to find the magnetic surfaces is as follows: First, a medium-sized surface (bold curve) in Fig. 1) is looked for by trial and error, at a fixed position of the electron source. The transit numbers N are established from the observed time differences. Then, a specific transit (e.g. N = 1 or 10, as indicated by the radial lines in the upper half of Fig. 1) is followed by moving the electron source vertically and maintaining the probe signal at the oscilloscope maximum by proper and simultaneous adjustment of the probe. This procedure allows to map a nest of surfaces within several hours. Observing about a dozen experimental points is sufficient to obtain the shape of a magnetic surface with an accuracy of about 1 - 2 mm. These points need not constitute a complete series of successive transits. As can be seen from the smooth shape of the outmost surface shown in Fig. 1, the separatrix is situated beyond the limiter aperture which is indicated by the dashed circle in the upper half of the figure.

For comparison, calculated magnetic surfaces are shown in the lower half of Fig. 1. The Garching version of the Gourdon field computation code [6] is used. There is good agreement between the shapes of the calculated and the experimental surfaces. A slight difference exists in the position of the magnetic axis which will be discussed later, in the section dealing with stray magnetic fields.

The rotational transform ι is defined as the ratio of transits N_θ/N in the limit of large N, where N_θ and N are the transit numbers the short and long way around the torus, respectively. It is obtained as part of the computer programme for the calculated surfaces, and is evaluated from the poloidal coordinates of the experimental points and the transit number N. Generally, values of N up to about 100 can be identified unabiguously, proving the linear relationship of N with the time difference between the source and the probe signals.

Two averaging procedures are used to minimize the residual influence of the poloidal position of the experimental points which still is present for $N \lesssim 20$:

i) The differences in poloidal angles between the points with transit number $N^+ \geq 1/2\ N_{max}$ are evaluated with respect to the first transit, and the sequence of ι_{N^+} obtained is averaged linearly;

alternatively and preferentially:

ii) Pairs of experimental points with transit numbers N_i and N_K are looked for which constitute as closely as possible an integer number of transits N_θ in the poloidal direction. The difference in poloidal angle between N_i and N_K still depends on the poloidal angle of the experimental points, for $N \lesssim 20$. Several pairs (N_i, N_K) therefore are analyzed at different poloidal positions, and the rotational transform is obtained as an average; the uncertainty of which is decreased by increased difference of $(N_i - N_K)$.

Using the second averaging procedure, Fig. 2 shows the rotational transform corresponding to the data of Fig. 1 vs. the vertical coordinate Z. The experimental points are connected by the bold curve; some error bars are entered. At Z = 5.5 cm (bold curve in Fig. 1) we find $\iota = 0.2315 \pm 0.0005$, increasing to $\iota = 0.2330$ at Z = 10 cm (equivalent to the limiter radius).

Throughout the investigation described in this paper, the magnetic surface shown as bold curve in Fig. 2 is measured several times in order to check the reproducibility. As an average over 10 observations we find for z = 5.5 cm $\iota = 0.2300 \pm 0.0007$, the error being the standard deviation of the data. This error is larger than the error of the experiment shown in Fig.1, due to long-term drifts which are believed to have been present during the course of this investigation.

For a linear stellarator having ℓ pairs of filamentary helix currents $\pm$ I at a pitch length $L = 2\pi R \frac{\ell}{m} \gg 2\pi r_H$, the rotational transform ι_f is given |3| as

$$\iota_f = \left(\frac{\mu_o}{\pi}\right)^2 \frac{\ell^2(\ell-1)}{m} r^{2\ell-4} \frac{R^2}{r_H^4} \left|\frac{I}{B}\right|^2 \qquad (1)$$

where B is the longitudinal (in our case toroidal) field, and r is a radial coordinate. The dependence on r drops out for $\ell=2$ which corresponds to a shear-free configuration in the approximation. The factor $(\mu_o/\pi)^2$ matches the unities of current, field, and radius in the above formula, r_H is the helix radius and R is the torus radius which is entered into this linear approximation via the pitch of the helix.

For a helix current distribution within a poloidal angle 2θ instead of filamentary currents, the rotational transform is reduced |7,8| to

$$\iota_\theta = \iota_f \left(\frac{\sin 2\theta}{2\theta}\right)^2 \qquad (2)$$

Taking the values of W VII A, this relation yields $\iota_\theta = 0.314 \cdot 0.738 = 0.232$ which is in good agreement with the experimental value of the standard case configuration.

In a toroidal $\ell=2$ stellarator a weak shear is present. Neglecting higher order terms in the inverse aspect ratio r/R, an analytic relationship |8| for the radial dependence of the rotational transform can be simplified as

$$\iota(r) = \iota_\theta + \delta\iota = \iota_\theta\left[1 + \left(\frac{m}{\ell}\frac{r}{R}\right)^2 (2 + 3{,}5\,\varepsilon^2)\right] \qquad (3)$$

where ε is the ellipticity of the almost elliptic magnetic surfaces. Using the data of W VII A for the standard case, ε is about 0.42 and an increase of $\delta\iota = 0.0088$ is obtained over a radial distance of r = 10 cm. This increase is much larger than the experimental one, see Fig. 2.

The lower curve in Fig. 2 is the rotational transform obtained by the field computation. The programme yields a value of $\iota = 0.215$ at $Z = 5$, being by 7 % lower than the average of our experiment. This discrepancy is larger than the experimental error and will be discussed next.

In the field computation the toroidal field is an analytic field $B = B_o R_o/R$. This field represents sufficiently the field produced by the 40 toroidal field coils of W VII A where the free bore of 1.1 m diameter is large as compared to the limiter aperture $2r_L \approx 28$ cm. The helix input data differ slightly from the data of the actual W VII A device, as specified in Table II.

Combining eq.(1) and (2) the rotational transform of an $\ell=2$ stellarator scales proportional to

$$\iota \sim \frac{1}{r_H^4} \left(\frac{\sin 2\theta}{2\theta} \right)^2 \qquad (4)$$

Entering the data of Table II into this relationship, we arrive at a correction factor of

$$\iota_c/\iota = \left(1.036^{+0.018}_{-0.036}\right) \cdot \left(1.077 \pm ?\right)$$

The accuracy of the second term is uncertain because of the somewhat arbitrary representation of the helix cross-section by filamentary conductors. Therefore, we estimate the correction factor to be $\iota_c/\iota = 1.12 \pm 0.05$ which yields a corrected rotational transform $\iota_c = 0.241 \pm 0.011$. This value is 5 % larger than the average of the experimental results, but just in agreement within the respective error bars.

CHANGE OF ROTATIONAL TRANSFORM

In a stellarator the rotational transform ι can be changed by changing the ratio of helix current I_{HX} to toroidal field coil current I_{TF}. In the experiments this ratio is varied between 0.83 and 1.69. The corresponding values of ι are shown in Fig. 3. The curve connecting the experimental values is the analytic approximation

$$\iota = 0.22 \left[\frac{I_{HX}}{I_{TF}}\right]^2 + 0.01 \left[\frac{I_{HX}}{I_{TF}}\right]^4 \qquad (5)$$

derived from the experimental data. In contrast to eq.(1), a 4th order term is to be included in order to obtain an appropriate fit. This term is caused by the torus curvature. A relationship similar to eq.(5) is valid also for the results of the field computations.

Fig. 4 gives the comparison of experimental surfaces at ι = 0.477 and 0.715 and computed surfaces. The latter are shown as thin lines. They agree well with the experiments (bold curves), if the respective coordinate systems are shifted by some mm. In both experiments the toroidal field points out of the figure and the electron beam is parallel to the field. Thus a clockwise rotation of the transit points is caused.

Details of the experiments at variable rotational transform and the accuracy of the results are listed in Table III and will be discussed next.

The first column in Table III gives the values of ι averaged from the experimental data as described above. The relative accuracy of ι is $\pm$ 0.2 %. The current ratio I_{HX}/T_{TF} is given in the second column. Note that I_{HX} is the current fed into the helix which has 4 windings per helical unit. The 40 toroidal field coils of W VII produces a field B = 1 T at a radius R_o = 2 m, energized by a current of I_{TF} = 10 kA. So, for comparison with eq.(1), the standard case I_{HX}/I_{TF} = 1 corresponds to $|I/B| = 4 \cdot 10^4$. [A turns / T]

In the experiments, in general only one generator is used, and the TF coils and the helix are connected in series. This has the advantage of temporal stability and low voltage ripple due to the high inductance of the TF system. For high ι the toroidal field coils are shunted by a water-cooled ohmic resistor. This couples the voltage ripple of the generator to the helix and introduces some uncertainty in the knowledge of the helix current, in addition to the accuracy of the dc measurements in the parallel branches of the TF coils and the TF shunt. As shown by the horizontal error bars of the experimental points in Fig. 3, this error increases with increased ratio I_{HX}/I_{TF}. The experiment at $I_{HX}/I_{TF} = 0.83$ is performed with a shunt parallel to the helix. Here one is essentially free of the generator voltage ripple and the error in the current ratio is low.

The results obtained in the standard field configuration at $I_{HX} = I_{TF}$ are averaged over 6 observations taken at a toroidal field of 0.25 T. The errors entered in the corresponding line of Table III are the standard deviations of the ensemble.

Generally, the major and minor diameters of the magnetic surfaces 2a and 2b, respectively, are evaluated within $\pm$ 0.2 cm. This introduces an error of about 10 % in the ellipticity ε which is listed as the last column of the table. In reference |8| formulae are given for ι and the ratio a/b vs. characteristic data of a ℓ=2 stellarator. These relationships can be simplified when neglecting higher-order terms in the inverse aspect ratio r/R and yield

$$\iota_\varepsilon = \frac{m}{2\ell}\,\varepsilon^2 \qquad (6)$$

Entering the observed values of ε, the values ι_ε of the above relationship and the experimental values only roughly agree, since the relative error of the diameters 2a, 2b is multiplied by a factor of 4 in this procedure.

On the other hand, the average radius of the surface $r = \sqrt{ab}$ is obtained with an accuracy of about 3 % experimentally. In this definition of the radius the magnetic surfaces are taken to be elliptic in shape and r is the radius of the circle covering the same area. At large values of r and especially at high rotational transform the shape of the surfaces deviates from an ellipse due to the torus curvature.

For a radial position close to the limiter aperture details of two magnetic surfaces are shown in Fig. 5. Although the absolute values of the currents in the system, i.e. the current in the TF coils and the current in the helix $I_{HX} = I_{TF} + I_S$ are known with an accuracy of $\delta I_{TF}/I_{TF} = 1\%$, the temporal stability of the current ratio is much better, $I_{HX}/I_{TF} = 1.0388 \pm 0.0003$. The two surfaces shown in Fig. 5 are composed from several sequences of transits, where the electron beam is directed both parallel and antiparallel to the magnetic field which is B = 0.2 T, directed out of the RZ-plane in the figure. For both surfaces, the sequences characterized by transit number N = 4i, i being integer, are entered in figure 5. These transits correspond to a beam directed parallel to the magnetic field and show a clockwise rotation in the RZ-plane.

They just fail to complete integer transits in the poloidal direction. This corresponds to a rotational transform slightly smaller than 1/4. Averaging the different sets of data, we find $\iota = 0.2491 \pm 0.0002$ for the outer surface, and $\iota = 0.2488 \pm 0.0001$ for the inner one. The errors are the standard deviation of the data sequences, the maximum deviation of a single sequence from the average is about twice this value. This is believed to be due to a residual effect of the gross poloidal position of the sequence, and of the residual variations in the currents, which are compensated by new settings of I_S, the additional current in the helix.

Note that in Fig. 5 the poloidal distance of, e.g. the transits N = 20 and 60, is smaller for the outer surface than for the inner surface, showing the increase in ι with radial position.

The amount of shear present in the W VII A stellarator field is evaluated from computed surfaces predominantly. The rotational transform increases weakly with the radial coordinate $r = \sqrt{ab}$, the increase being strongly dependent on the value of ι itself. Several analytical relationships are tried to fit the computed data of $d\iota/dr$. For values of r between 3 and 9 cm and ι between 0.2 and 0.7 the relationship

$$d\iota/dr \left[cm^{-1}\right] = 10^{-3} \cdot r^{1.2}\, \iota^{2.7} \qquad (7)$$

represents the computed values within 20 %, as shown in Fig.6. When increasing ι above 0.7, the size of the separatrix is reduced considerably, and $d\iota/dr$ increases stronger than the 2.7^{th} power.

Eq. (7) contrasts largely with the corresponding relationship obtained from the analytic formula of the linear stellarator, eq. (3). There $d\iota/dr$ is proportional to r and ι.

The experimental data of $d\iota/dr$ as functions of r and ι scatter largely for the observed surfaces at large values of ι. This is presumably caused by drifts in the current systems. For the standard case configuration, the values of $d\iota/dr$ are larger by a factor of about 1.5 than the computed ones.

In the stellarator field without large plasma current the plasma radius is given by the magnetic surface just touching the limiter aperture r_L. If we characterize the surfaces by their maximum and minimum diameters 2a and 2b, respectively, from the experiments and from the field computation, we arrive at an approximately linear relationship between the ratio a/b and the rotational transform ι. This relationship linearizes the published /8/ dependence and is valid for the range $0.15 \leq \iota \leq 0.72$ within about 3 % of the coefficients as

$$\iota = -0.73 + 0.61\ a/b \qquad (8)$$

The effective plasma radius r_p then is related to the limiter radius by

$$r_p = r_L \sqrt{\frac{0.61}{\iota + 0.73}} \qquad (9)$$

as shown in Fig.7. Since in W VII A the limiter consists of 4 sectors of about 90° which are vertically adjustable within 10 mm, in Fig.7 two curves are given, labelled "limiter out" and "limiter in". In this lower curve an additional offset of the magnetic surface is also taken into account. Beyond $\iota = 0.8$ these curves are dashed. In this region the shape of the computed surfaces increasingly deviates from the almost elliptic shape with increasing r and ι. The dotted curve in Fig.7 marked "separatrix" indicates the steep reduction of the plasma radius when, at still higher ι, the size of the separatrix becomes smaller than the limiter aperture. As an example, for $\iota = 1$ the plasma radius is reduced to 5 cm, according to computed surfaces.

In the stellarator field without large plasma current the plasma radius is given by the magnetic surface just touching the limiter aperture r_L. If we characterize the surfaces by their maximum and minimum diameters 2a and 2b, respectively, from the experiments and from the field computation, we arrive at an approximately linear relationship between the ratio a/b and the rotational transform ι. This relationship linearizes the published /8/ dependence and is valid for the range $0.15 \leq \iota \leq 0.72$ within about 3 % of the coefficients as

$$\iota = -0.73 + 0.61\ a/b \qquad (8)$$

The effective plasma radius r_p then is related to the limiter radius by

$$r_p = r_L \sqrt{\frac{0.61}{\iota + 0.73}} \qquad (9)$$

as shown in Fig.7. Since in W VII A the limiter consists of 4 sectors of about 90° which are vertically adjustable within 10 mm, in Fig.7 two curves are given, labelled "limiter out" and "limiter in". In this lower curve an additional offset of the magnetic surface is also taken into account. Beyond $\iota = 0.8$ these curves are dashed. In this region the shape of the computed surfaces increasingly deviates from the almost elliptic shape with increasing r and ι. The dotted curve in Fig.7 marked "separatrix" indicates the steep reduction of the plasma radius when, at still higher ι, the size of the separatrix becomes smaller than the limiter aperture. As an example, for $\iota = 1$ the plasma radius is reduced to 5 cm, according to computed surfaces.

EXTERNAL FIELDS

In a stellarator external radial and/or vertical magnetic fields $B_\perp$ produce a vertical and/or radial shift Δ of the magnetic axis which is given, e.g. in ref.[3] as

$$\Delta = \frac{B_\perp}{B_o} \cdot \frac{R_o}{\iota} \qquad (10)$$

The magnetic axis is recognized to be the center of magnetic surfaces, in the limit of vanishing size of the latter. When interpretating the magnetic axis as center of a surface of finite dimension, one has to compromize with the size of the latter: if it is too small, the relative error of the evaluation is large, if it is too large, nonlinearities may cause false conclusions. Therefore, we would like to regard a dimension $r = \sqrt{ab} = 5$ cm as reasonable.

Computed values corresponding to this surface for the standard case W VII A configuration are listed in Table IV. They agree within 10 % with the result of eq.(10). Note that in the absence of external fields the offset of the center of the surface is increasing weakly with the size of the latter to about R_o - 1.2 cm for the surface just touching the limiter aperture, $r \approx 10$ cm.

With external fields $B_\perp$, the shift of the axis is proportional to the ratio $B_\perp/B_o$. Note that for e.g. a positive direction of the toroidal field a radial field produces an upward offset of the axis, whereas a vertical field pointing downward ($B_Z < 0$) shifts the axis radially outward.

In addition to this shift, the center of the surfaces shows a rotation in the RZ-plane when following the azimuthal coordinate, the amplitude being about 20 % of the observed shift.

From the data analyzed it appears that this rotation still is present in the limit of vanishing dimension of the magnetic surfaces, corresponding to a helical magnetic axis produced by the external fields. At the position of the experimental ports the phase of the helical magnetic axis is such that it corresponds to a vertical (radial) oscillation introduced by the vertical (radial) external field which changes sign at successive port planes. The positive sign always corresponds to a surface with the long side directed between the radial and the upper vertical port, dependent on the sign of the ratio of $B_\perp/B_o$ and the port number, as already discussed along with the systematics of the W VII A field topology.

The rotational transform is changed significantly in the case of a vertical field, the change being proportional to $-B_z/B_o$. This can be understood qualitatively the following way: The outward shift of the magnetic axis causes a lower toroidal field being active, due to the 1/R dependence of the toroidal field. Quantitatively, however, the increase $\delta\iota$ given in Table IV is larger than a value corresponding to the relation of ι and the ratio of helical to toroidal currents, eq. (5).

The radial field studied in comparison was chosen to have approximately the same 1/R dependence as the toroidal field. This is achieved considering two current loops with opposite currents at radii of 1.2 m at vertical positions Z = $\pm$ 2 m. No change of t is expected since the vertical shift introduces no change in the toroidal field. Outside the mid-plane of the torus small vertical components exist in the field of the chosen current configuration. They cancel after several revolutions of the field line.

STRAY FIELDS

Three types of experiments are performed in order to obtain evidence of the presence and scaling of stray magnetic fields in the W VII A installation:

- disconnecting the helix and observing the motion of the beam electrons at variable toroidal field,

- varying the toroidal field at constant field topology of the stellarator configuration and observing the position of the magnetic axis,

- superimposing to the stellarator configuration a local radial field of variable strength and polarity.

In the case of a pure toroidal field charged particles show a vertical drift. Using standard notation, the drift velocity amounts to

$$V_D = \frac{m}{eB}\frac{1}{R}\left(\frac{1}{2} V_\perp^2 + V_\parallel^2\right) \qquad (10)$$

For electrons this drift is directed upwards if the magnetic field B is antiparallel to the toroidal coordinate, irrespective of the direction of the velocity. Entering the data of our experiment, a vertical offset $\Delta_Z = 0.1$ cm is caused by a toroidal field of B = 0.1 T during one transit of the beam the long way around the torus.

An additional vertical field B_Z changes the pitch of this motion, and an additional radial field B_R causes the electrons to spiral radially, according to

$$B_{R,Z} = \frac{B}{2\pi R} \cdot \Delta_{R,Z} \qquad (11)$$

where Δ_R, Δ_Z are the radial and vertical offsets introduced after one transit the long way around the torus.

Some results of the experiments are shown in Fig. 8. The upper string of transits corresponds to a field of $B_o = -0.25$ T, whereas the lower one is taken at a different position of the electron source and at a field of $B_o = -0.1$ T. In the figure, the toroidal fields are pointing out of the RZ-plane and the electrons drift upwards. The dots (circles) correspond to electrons directed parallel (anti-parallel) to the field.

In the upper half of the figure, the thin lines connecting the experimental points clearly demonstrate the electron drift. The ratio of the stray fields B_Z/B_R follows directly from the slope of the dashed line. Close inspection of the distance of neighbouring transit points reveals a slight increase with increasing R, consistent with stray fields $B_R = -1.1 \cdot 10^{-4}$ T and $B_Z = -0.53 \cdot 10^{-4}$ T being constant over the radial distance between R = 195 and 205 cm, when one considers also the toroidal field varying proportional to 1/R. The lower curve in Fig. 8 yields stray fields $B_R = -0.57 \cdot 10^{-4}$ T and $B_Z = -0.75 \cdot 10^{-4}$ T at a toroidal field B = - 0.1 T. The experimental error in the stray fields is about 1 % since the positions of several transits are averaged.

Observing the change of the position of the magnetic axis as function of the applied field, when keeping the ratio of currents in the helix and the toroidal field coils constant, yields information on stray fields via eq. (10). Here the experimental error is larger than in the first method. In the standard case of the W VII A stellarator field, experimentally both radial and vertical offsets of the center of the typical magnetic surface with $r = \sqrt{ab} = 5$ cm are observed, dependent on the magnitude but not on the polarity of the toroidal field. The data are listed in Table V. The calculated radial offset of 0.6 cm present already in the absence of external fields is taken into account. The resulting vertical and radial fields are entered in the Table along with the experimental error.

These results are compared with the results obtained in the experiments without helix current in Fig. 9. The upper half gives the radial and the lower half the vertical stray fields, vs. the applied toroidal field. The dots correspond to the experiments without helix current and the circles are fields obtained from the position of the magnetic axis. Within the experimental error indicated by the errors bars and shown as dashed lines in the figure, the data obtained in both types of experiments agree.

In the average, the observed stray fields are proportional to the toroidal field. This can be understood qualitatively if one considers the construction of the current supply of the W VII A toroidal field coils [9]. The current supplies can be approximated by two loops with opposite currents placed about 1.1 m above the torus mid-plane at radii of 1.6 and 1.8 m, respectively. These current loops are interrupted by the toroidal field coils. Estimating this effect, we arrive at radial and vertical stray fields of $0.20 \cdot 10^{-4}$ T and $-0.14 \cdot 10^{-4}$ T at a toroidal field of 0.1 T produced by the current supply. These fields have the correct sign but are lower by factors of about 2 as compared to the experiment. Additional radial and vertical stray fields of the same order can be argued also if one considers an azimuthal or vertical offset of one toroidal field coil by 1 - 2 mm.

Whether the stray fields shown in Fig. 9 are proportional to the toroidal field up to the design value is not clear. Only little information exists of the permeability of the materials used at and close to the W VII A installation, and still less is known of its field dependence. Distortions of the coil and helix structure due to magnetic forces were found to be reasonably small up to fields of 2.5 T and should have no effects on the field topology. Assuming the stray fields to be proportional to the toroidal field, at

B_o = 2.5 T being presently used in the W VII A plasma experiments |10|, stray fields of the order of $5 \cdot 10^{-3}$ T are expected, whereas the plasma current observed to exceed 30 kA produces a poloidal field of about 10 times this value.

For further study of the effects of stray fields on the stellarator configuration W VII A, in a third type of experiments a local and predominantly radial field is superimposed to the standard W VII A stellarator field. This local field is produced by a coil arrangement about 40 cm radially outward of the minor torus axis, close to the helix. The axis of the coil arrangement is declined 6^o below the mid-plane of the torus. The axial field component of this coil arrangement introduces a predominantly radial field up to $\pm$ 2 % of the toroidal field of the stellarator, which drops to half of its center value within a (vertical or azimuthal) distance of about 25 cm. The effect of this inhomogeneous field into the magnetic surfaces is also calculated for comparison with the experiment.

The experiments are performed as follows: First, the standard case configuration is established and the position of about a dozen transits is recorded. Then the current in the external coil is increased in small steps and the motion of a specific transition point is followed by the probe. Fig.10 shows the nest of magnetic surfaces thus obtained.

No break-up or distortion of the magnetic surfaces is observed, apart from the expected, predominantly vertical, shift of the magnetic axis. In Table VI a comparison is made of experimental and computed values of the observed position of the axis and of the magnitude of the rotational transform when applying local radial fields directed outwards and inwards. Note that the polarity of the toroidal field differs in the experiments and the computation. Therefore,

the vertical shift of the axis is downwards in the experiment and upwards in the computation when applying an outward (positive) radial field. Since the magnetic field of the coil system is not symmetric with respect to the position of the magnetic surfaces, also a radial shift of the surfaces and a change in the rotational transform is observed, both for computed and for measured surfaces. When the superimposed field is predominantly radially outward, the additional radial shift is inward and ι is increased, apparently irrespective of the polarity of the toroidal field, see Table VI. The change in ι is larger in the experiment than in the computation.

RATIONAL VALUE OF ROTATIONAL TRANSFORM

It is well known, e.g. /6,11/, that magnetic islands are introduced in a stellarator field by external disturbances of the toroidal or helical field systems. Therefore a large fraction of the experimental time was dedicated to the investigation close to the rational value $\iota = 1/4$ of the rotational transform. As already discussed in the context of Fig. 5 , where details of surfaces with a major diameter comparable to the limiter aperture are shown, the temporal stability of the currents in the field systems is of major importance in the case of a low-shear configuration. Close to the rational value of ι the distance of the transits characterized by the transit number $(p+1/\iota)$, $p = 0,1$, etc. is small. Since - dependent on the base pressure in the torus - only a limited number of transits can be recorded, a magnetic surface is to be composed from data obtained by different setting of the electron source.

Furthermore, the electron beam is to be shifted radially off the electron source by an electric field transverse to the magnetic field in order to avoid the absorption of the beam by the source after the first transit in the poloidal direction. In some cases this electric field introduced an erroneous offset of later transits passing closely by the electrodes, due to the stray field of the latter. These data were not used in the evaluation.

Fig. 11 is a compilation of the results obtained under conditions regarded sufficiently constant and reliable. Several magnetic surfaces are recorded partially and are characterized by their average rotational transform. The value $\iota = 1/4$ is seen as the cross-over of the dashed radial positions of the pairs of transits 1 and 17 as well as 4 and 20. Note that the rotational transform evaluated from the two arcs of the outmost surface still shows a slight dependence on the poloidal position which - at a position radially outward - yields the higher value. For the two arcs of the inner surface at $\iota < 1/4$ this feature is reversed and the outside arc gives a slightly lower value. The arcs labelled 0.2495 and 0.2498 are similar in shape to those of Fig. 5. A magnetic island, however, could not be identified experimentally.

Earlier, we had calculated |1| the magnetic disturbances which are produced by certain construction elements of the W VII A helix, called the helix steps |1| . They produce magnetic islands only at rational rotational transforms, at t = 1/4 with a radial width of about 3 cm, equivalent to less than 25 % of the limiter radius. This field pattern is reproduced in the upper half of Fig. 12. When taking also the currentleads of the W VII A helix into account, a rotation of the island structure is observed and the radial dimension of the islands is approximately the same as in the first case. The gross shape of these islands and the experimentally observed arcs of magnetic surfaces, Fig. 11, do not seem to be contradictory, although no fit could be achieved.

As compared to the upper half of Fig. 12 the lower half shows an island structure with much smaller radial dimension. Here a torsatron configuration is calculated for the W VII A geometry including also the disturbance by helix steps. Only one half of the helix is energized to the value of the design current of 40 kA. A compensating vertical field of

0.06 T is present at a toroidal field of 2.2 T. Torsatrons usually show a higher shear than stellarators at identical values of the rotational transform. /6/. This is also the case of the W VII A torsatron field, as compared to the W VII A stellarator field. The higher shear of the torsatron configuration reduces the size of the magnetic islands effectively, as expected.

CONCLUSIONS

Combining the experimental results of this investigation and the data obtained from numerical computation the following conclusions are drawn for the stellarator configuration of W VII A.

- There is good agreement between the shape of experimental and computed magnetic surfaces and the magnitude of the rotational transform agrees within about 5 %. The experimental value of ι is considered to be more precise than the computed one.

- Nested magnetic surfaces are shown experimentally to exist within the limiter aperture for $\iota < 1/4$. The separatrix remains outside the limiter aperture for $\iota < 0.8$, according to computation.

- Stray magnetic fields appear to be mainly proportional to, and amounting to about 0.4 % of, the toroidal field.

- At $\iota = 1/4$ magnetic islands caused by the fields of structural elements of the helix conductors are calculated to have a radial dimension of less than 25 % of the limiter radius. They could not be identified experimentally.

- The magnetic islands would be considerably reduced in size in a torsatron configuration of W VII A, due to the increased shear of the latter.

ACKNOWLEDGEMENTS

The authors wish to express their thanks to the discussions they had with their colleagues at the Institute, especially with Drs. G. Grieger and H. Wobig. They are grateful to the technical teams operating the W VII A facility as well as the energy supply, and to Mrs. V. Welge for performing numerous field computations.

REFERENCES

|1| Proc.8th SOFT, Noordwijkerhout, EUR 5182 e, 75 (1974), p. 65 and p. 235.

|2| R.M.Sinclair et al, Rev.Sc.Instr. 41, 1552 (1970)

|3| e.g. K.Miyamoto, Phys.Fl. 14, 722 (1971)

|4| A. Gibson and J.B. Taylor, Phys.Fluids 10, 2653 (1967)

|5| S.Rehker, private communication

|6| G.Gourdon, e.g. in Proc.Third Int.Conf.of Plasma Phys. and Contr. Fus.Research 1968 (Novosibirsk), IAEA, Vienna 1969, p. 847

|7| A.I.Morozov and L.S.Solovev, Rev.of Plasma Physics 2,57; Consultants Bureau, New York (1966); cited in:

|8| E.D.Andrukhina et al., Proc.P.N. Lebedev Institute, 65,69; Consultants Bureau, New York (1974)

|9| As |1| , page 109

|10| W VII-A Team, paper contributed to 6th Conf.on Contr. Nucl.Fusion Res., Berchtesgaden 1976

|11| As |1| , page 221.

TABLE I: Construction Data of the W VII A Stellarator

Torus	Major radius R_o = 2 m, limiter radius r_L ≈ 14 cm Vertical and radial ports, diameter 10 cm, situated every 36° in azimuth φ
Toroidal Field	40 coils, low magnetic ripple Free bore 1.1 m diameter Toroidal field at R_o: B_o = 0.1 T at I_{TF} = 1 kA Current I_{TF}: pulsed up to 40 kA, this investigation: dc up to 2.5 kA
Helix	Poloidal index ℓ = 2, toroidal index m = 5 4 windings per helical unit in counter-clockwise direction Poloidal width 54° Radial width 4 cm Average helix radius r_H ≈ 23 cm Current I_{HX}: pulsed up to 40 kA, this investigation: dc up to 2.5 kA

TABLE II: Comparison of Helix Data

	W VII-A device	Computation input
average helix radius r_H	22.6 $^{+0.2}_{-0.1}$ cm	22.8 cm
helix construction	4 bundles of 4 parallel conductors	-
helix representation	-	5 filaments at average poloidal angles of 0, ± 12, $\pm 24^\circ$
poloidal width 2θ	$54^\circ \pm 0.2^\circ$	

TABLE III: Variation of Rotational Transform

	Exp.rot. transform averaged ι	current ratio I_{HX}/I_{TF}	diameter of magnetic surface (cm) 2a	2b	average radius(cm) $r = \sqrt{ab}$	ellipticity $\varepsilon = \frac{a^2-b^2}{a^2+b^2}$
	0.1524	0.828 $\pm$0.004	11.8	8.0	4.9	0.36
standard case	0.2300 $\pm$0.0007	1.000 $\pm$0	12.9 $\pm$0.1	8.2	5.14	0.42 $\pm$0.02
	0.2463	1.036 $\pm$0.002	12.4	7.8	4.9	0.43
	0.3256	1.179 $\pm$0.004	8.8	4.8	3.3	0.54
	0.3348	1.196 $\pm$0.004				
	0.477	1.424 $\pm$0.014	9.7	5.3	3.6	0.54
	0.715	1.686 $\pm$0.025	9.2	3.8	3.0	0.71
accuracy $\pm$0.2 %			$\pm$ 0.2 cm		$\pm$ 3 %	$\pm$10 %

TABLE IV: Effects of External Fields onto the W VII A Standard Case Stellarator Field (Computation)

External field	Magnetic axis Center of magn. surface with r = $\sqrt{ab}$ = 5 cm		Rotational transform		
	radial	vertical	ι	+	$\delta\iota$
$B_R=B_Z=0$	R_o-0.6 cm	0 cm	0.215		0
vertical homogeneous $B_Z/B_o = -10^{-3}$	outward shift + 1 cm	oscillation amplitude $\pm$ 0.2 cm	0.215		+0.007
radial, approx. prop. 1/R $B_R/B_o = +10^{-3}$	oscillation amplitude $\pm$ 0.2 cm	upward shift + 1 cm	0.215		small

TABLE V: Stray Vertical and Radial Fields Evaluated from Center of Magnetic Surface r ≈ 5 cm; W VII-A Standard Case Field Configuration

Toroidal field	Observed shift		Stray field		
	radial	vertical	vertical	radial	
B_o[T]	[cm]		[10^{-4} T]		
0.25	1.2	0.36	-3.5 ±0.2	1.0 ±0.1	
0.25	0.27	0.35	-0.8 ±0.2	1.0 ±0.1	
0.25	0.23	0.30	-0.7 ±0.2	0.9 ±0.1	both
0.25	0.34	0.4	-1.0 ±0.3	1.2 ±0.2	beam
-0.25	0.2	0.25	0.6 ±0.2	-0.7 ±0.1	directions
-0.25	0.2	0.36	0.6 ±0.3	-1.0 ±0.2	
-0.25	-0.15	0.4	-0.4 ±0.2	-1.2 ±0.1	
-0.035	-0.7	1.05	-0.3 ±0.1	-0.4 ±0.05	drift surface
-0.035	-0.35	1.1	-0.14±0.05	-0.44±0.02	averaged
-0.035	-0.15	0.85	-0.06±0.05	-0.34±0.02	
-0.25	0.05	0.35	+0.2 ±0.4	-1.1 ±0.3	3 points;
-0.15	-0.03	0.38	-0.05±0.2	-0.7 ±0.2	surface
-0.1	-0.1	0.47	-0.1 ±0.2	-0.5 ±0.1	taken as
-0.05	-0.33	0.73	-0.2 ±0.1	-0.4 ±0.1	ellipse
-0.03	-0.65	1.0	-0.2 ±0.05	-0.4 ±0.1	

TABLE VI: Local Field Superimposed to Standard Case W VII-A Configuration

	Position of center of magn. surface				rotational transform ι	
	vertical (cm)		radial (cm)			
	exper.	comput.	exper.	comput.	exper.	comput.
radial field [T]						
$+5 \cdot 10^{-3}$	-0.15	+0.7	-0.9	-0.8	0.2300	0.2159
0	+0.55	0	-0.65	-0.6	0.2276	0.2148
$-5 \cdot 10^{-3}$	+1.1	-0.5	-0.5	-0.2	0.2257	0.2138
toroidal field [T]	-0.25	+0.25	same		same	

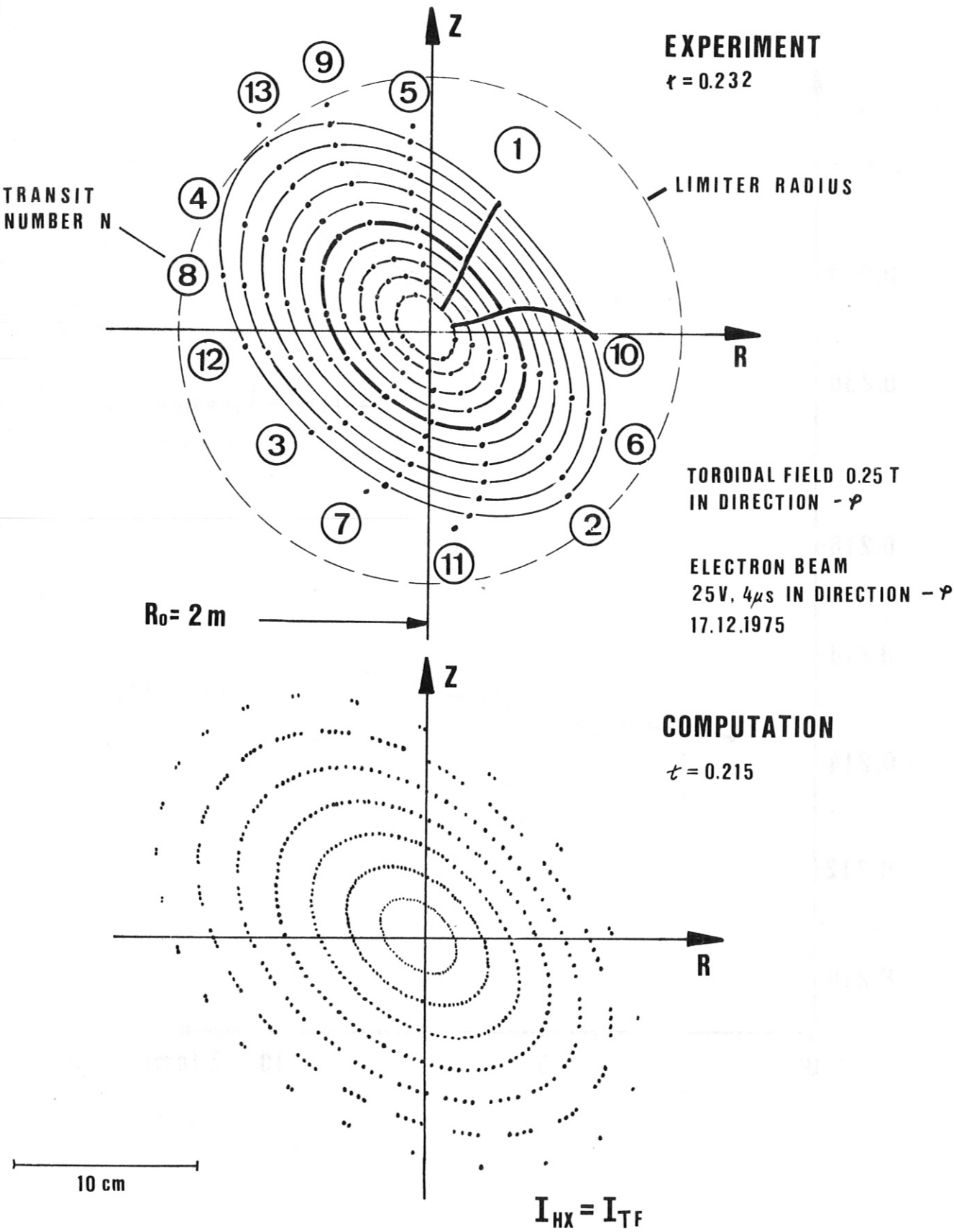

Fig. 1: Comparison of experimental and computed magnetic surfaces of stellarator W VII A standard case field configuration ($I_{HX} = I_{TF}$)

ROTATIONAL TRANSFORM VS VERTICAL COORDINATE

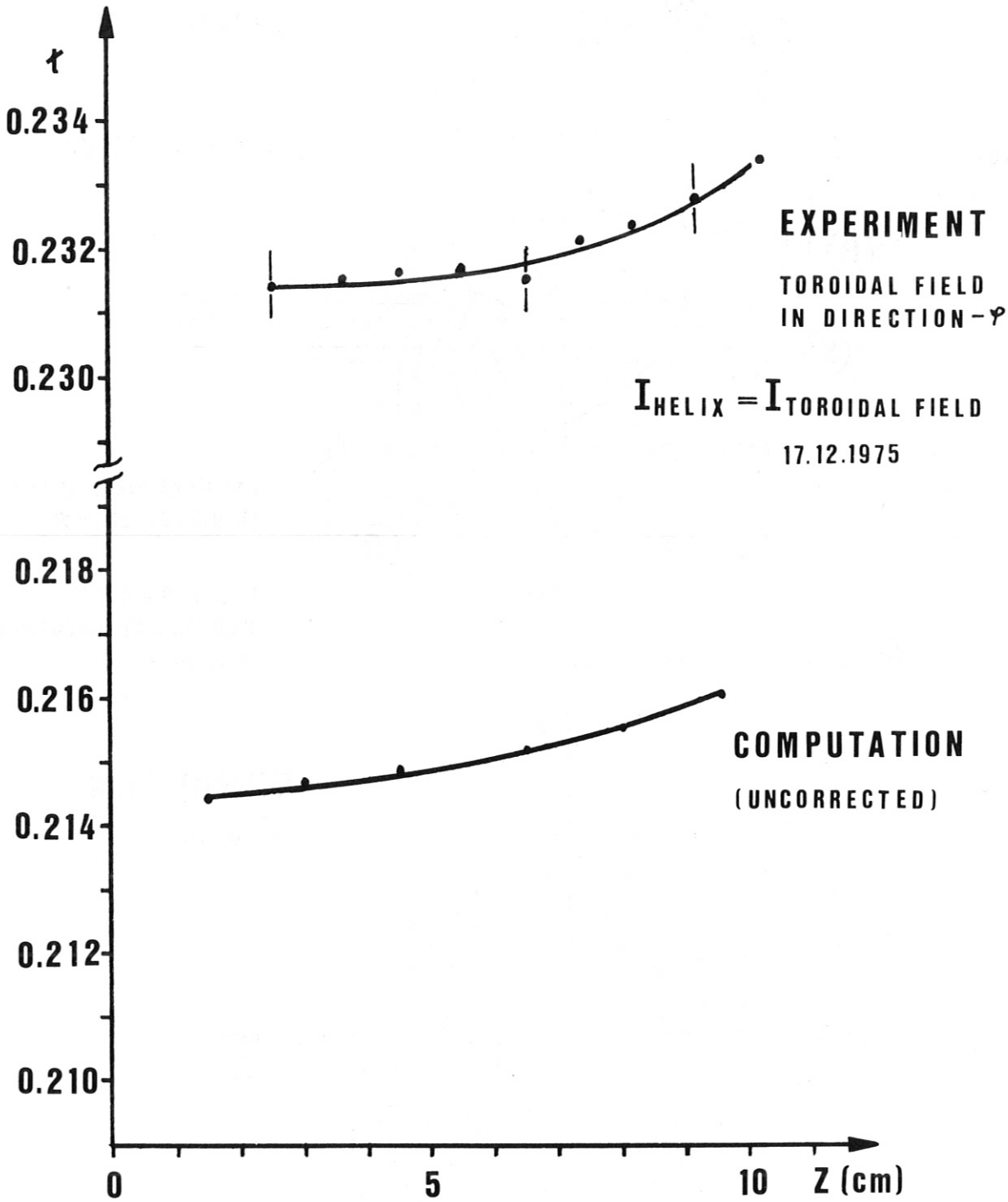

Fig. 2: Dependence of rotational transform on the vertical co-ordinate, standard case configuration.

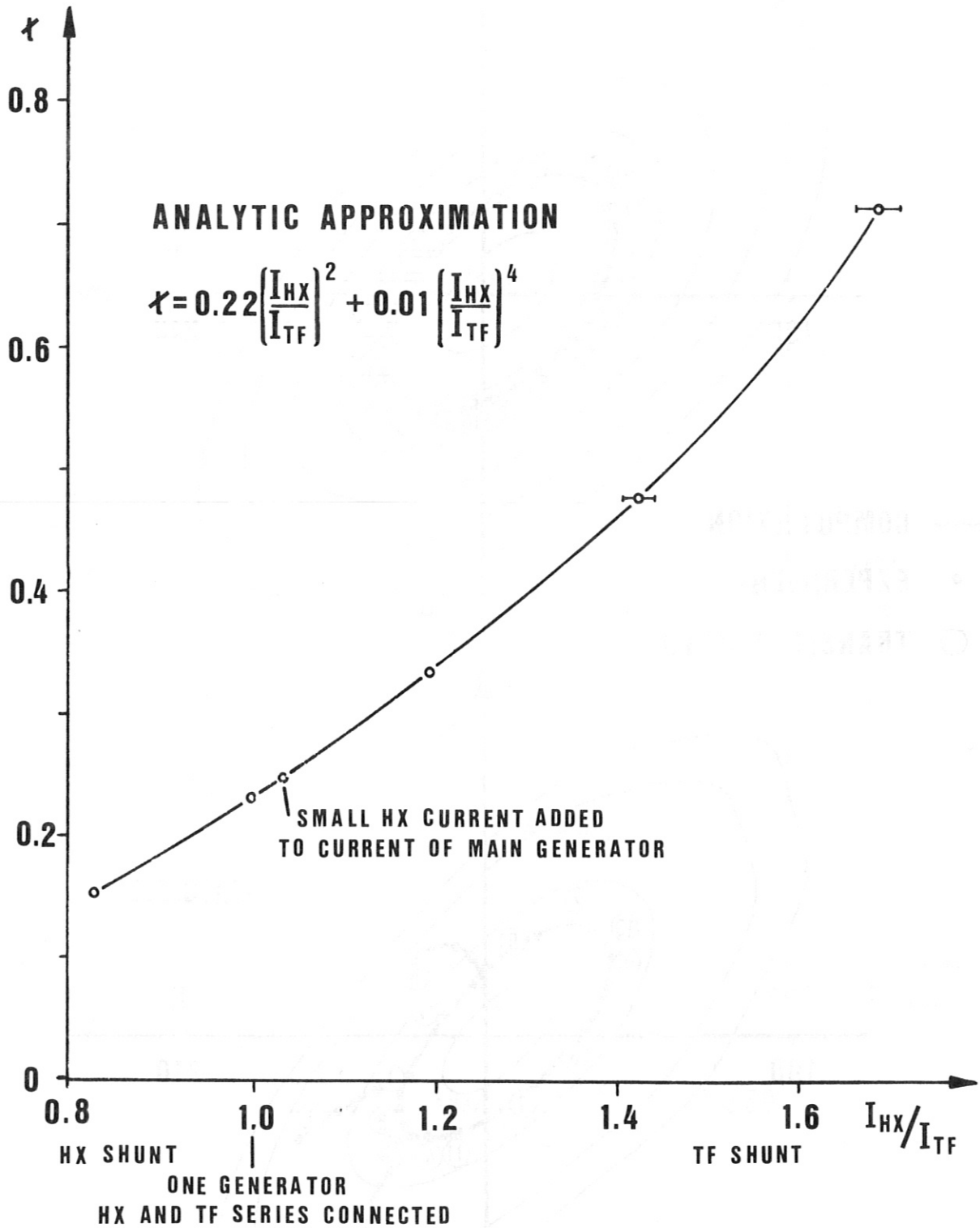

Fig. 3: Variation of rotational transform by changing the current ratio I_{HX}/I_{TF} and analytic fit of the relationship obtained experimentally.

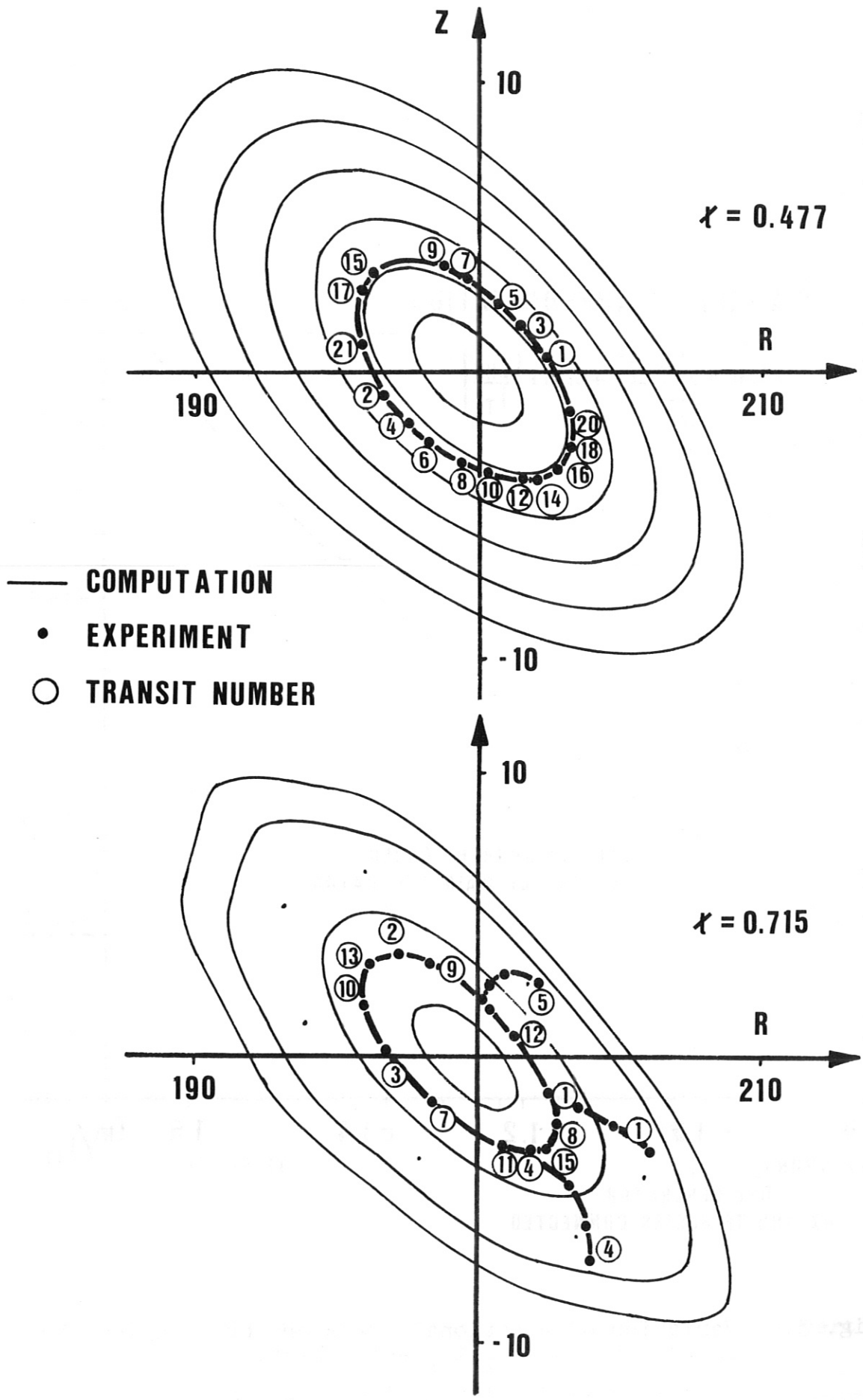

Fig. 4: Comparison of experimental and computed magnetic surfaces at elevated values of rotational transform.

DETAILS OF SURFACES CLOSE TO LIMITER APERTURE

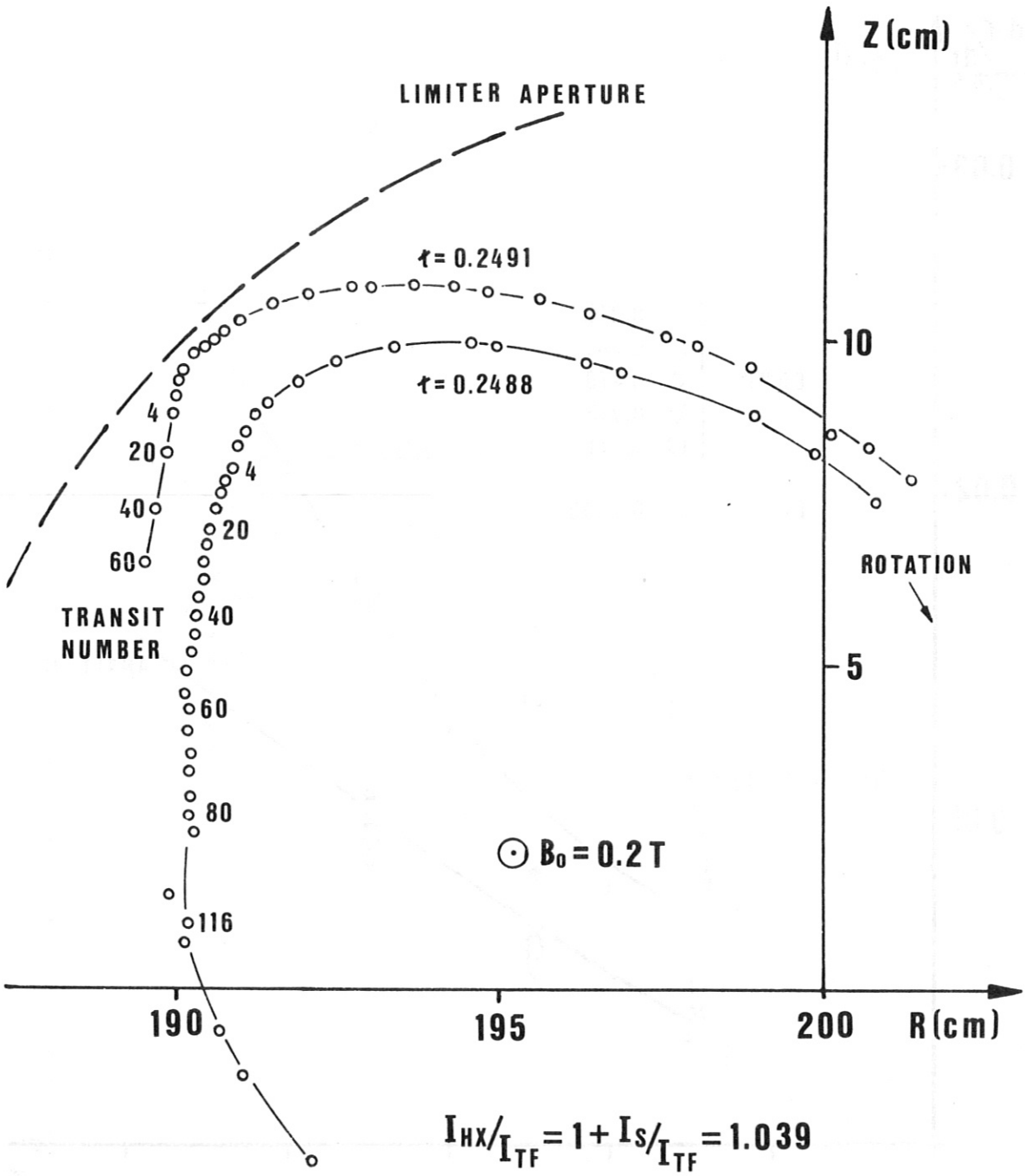

Fig. 5: Details of magnetic surfaces radially close to the limiter aperture at $t \lesssim 1/4$.

ANALYTIC FIT OF $\frac{d\iota/dr}{\iota^{2.7}}$ VS $r=\sqrt{a\cdot b}$

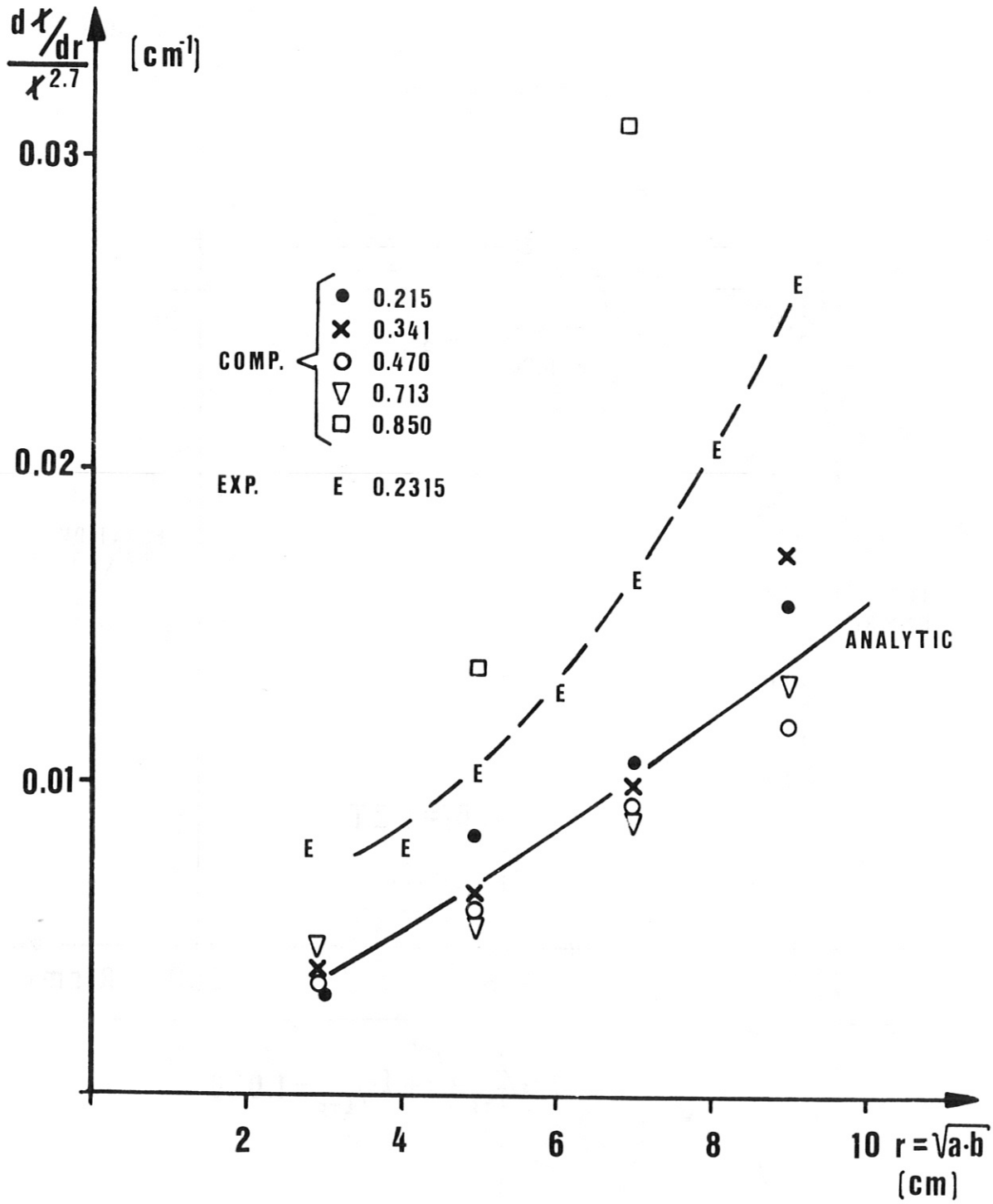

Fig. 6: Analytic fit of computed and experimental values of $\frac{d\iota/dr}{\iota^{2.7}}$ as function of average radius $r=\sqrt{ab}$ of the magnetic surfaces characterized by their major and minor radii a and b, respectively.

PLASMA RADIUS VS ROTATIONAL TRANSFORM

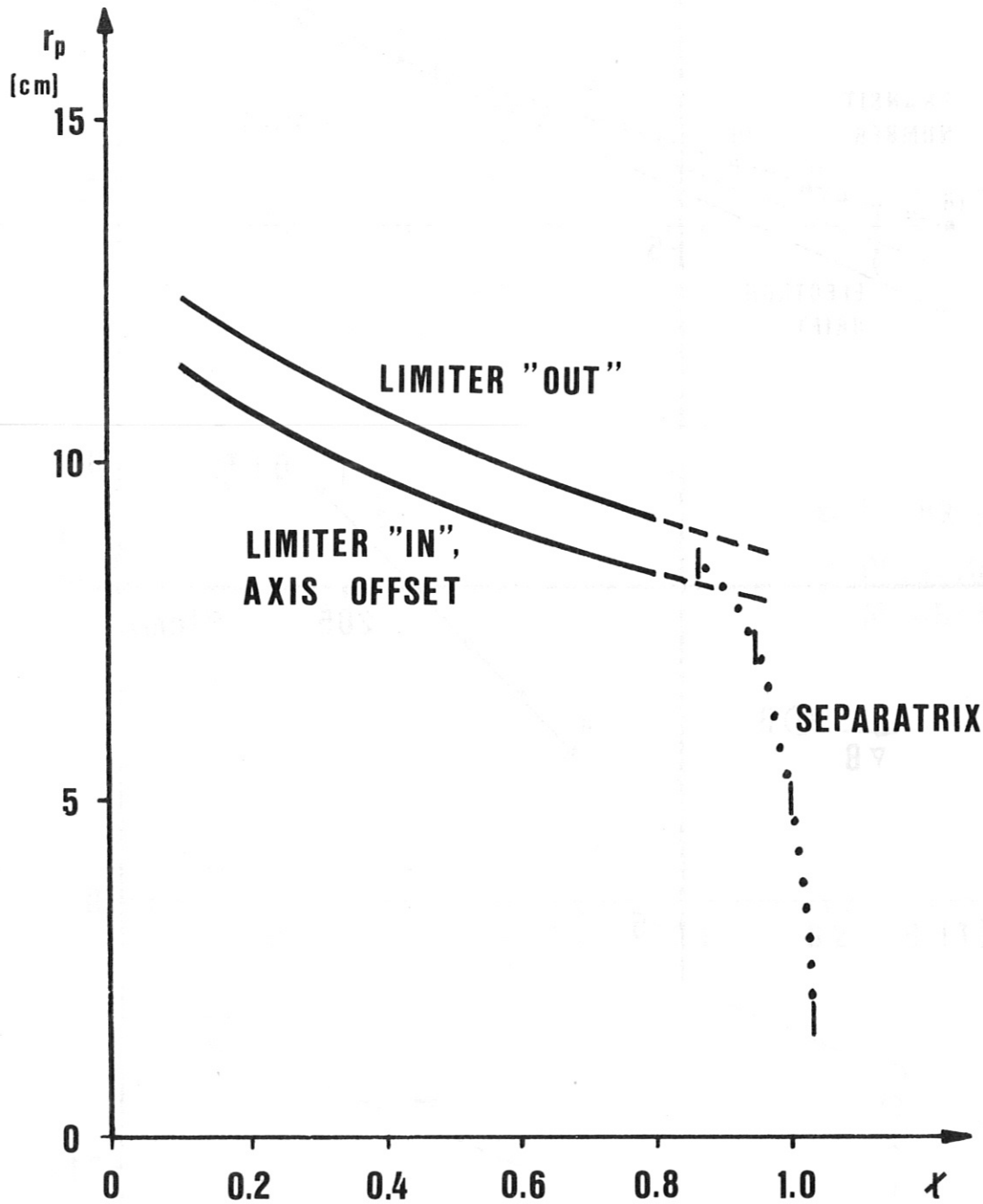

Fig. 7: Plasma radius $r_p = \sqrt{ab}$, $a \to r_L$, as derived from linearized relationship $\iota(a/b)$, for positions of LIMITER OUT and LIMITER IN; in the latter case observed offset of magnetic axis also taken into account. At large ι reduced plasma radius due to reduced size of the separatrix.

POSITIONS OF TRANSITS WITHOUT HELICAL FIELD

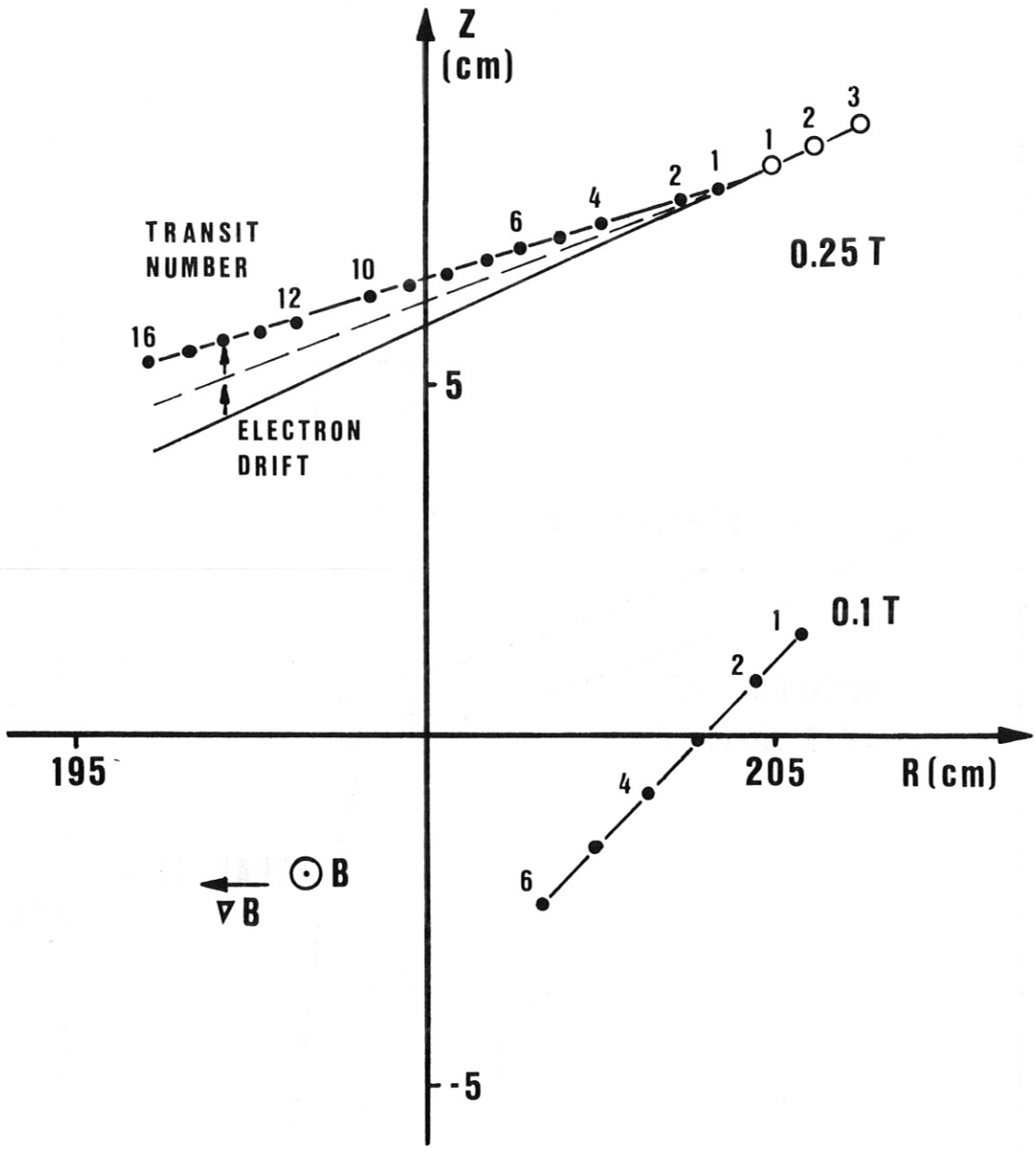

Fig. 8: Observed drift of electron beam by torus drift and stray radial and vertical fields.

STRAY RADIAL UND VERTICAL FIELDS

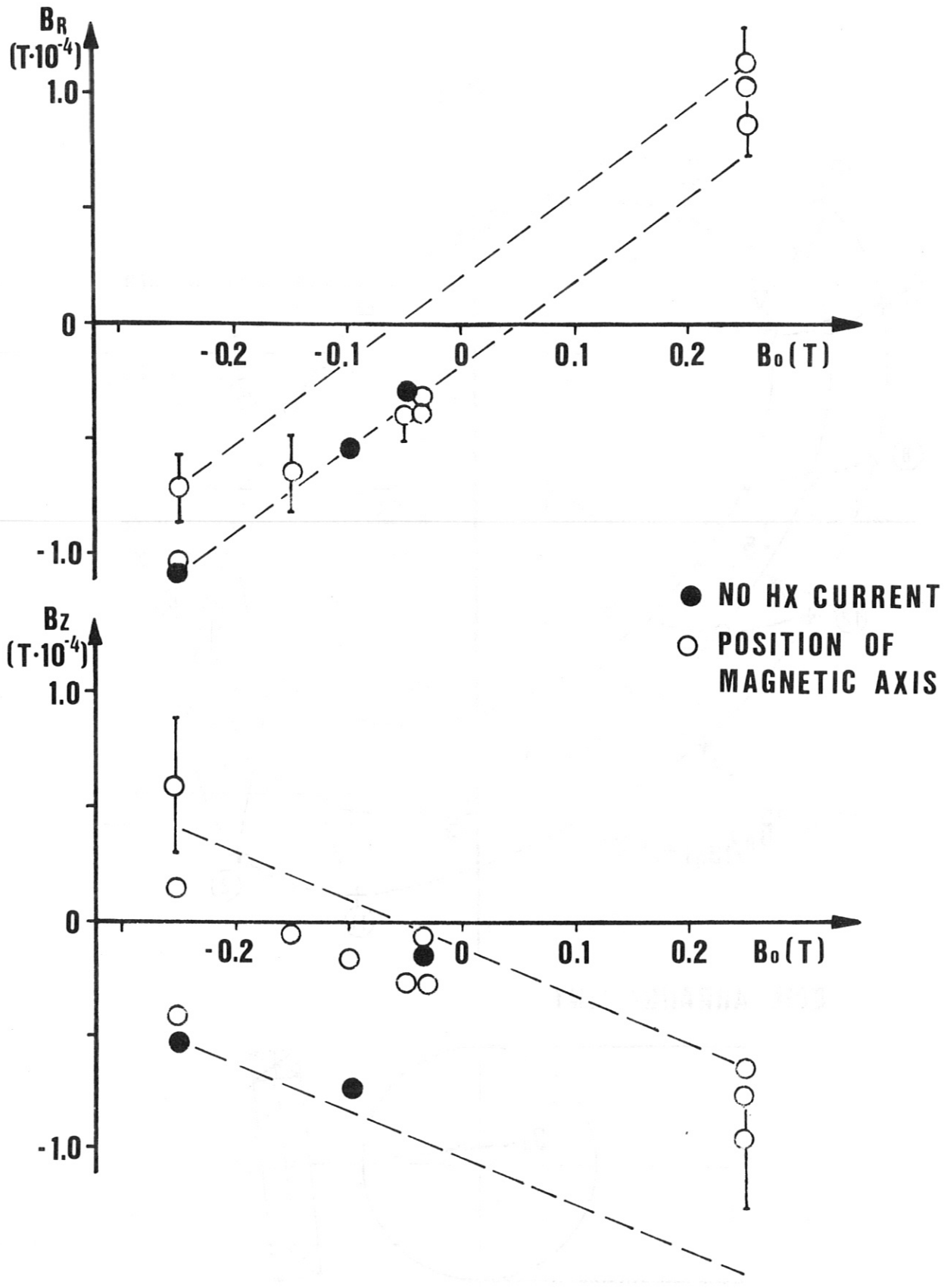

Fig. 9: Stray radial and vertical fields as derived from experiments without helix current and from the observed shift of the magnetic axis.

SUPERIMPOSED LOCAL FIELD

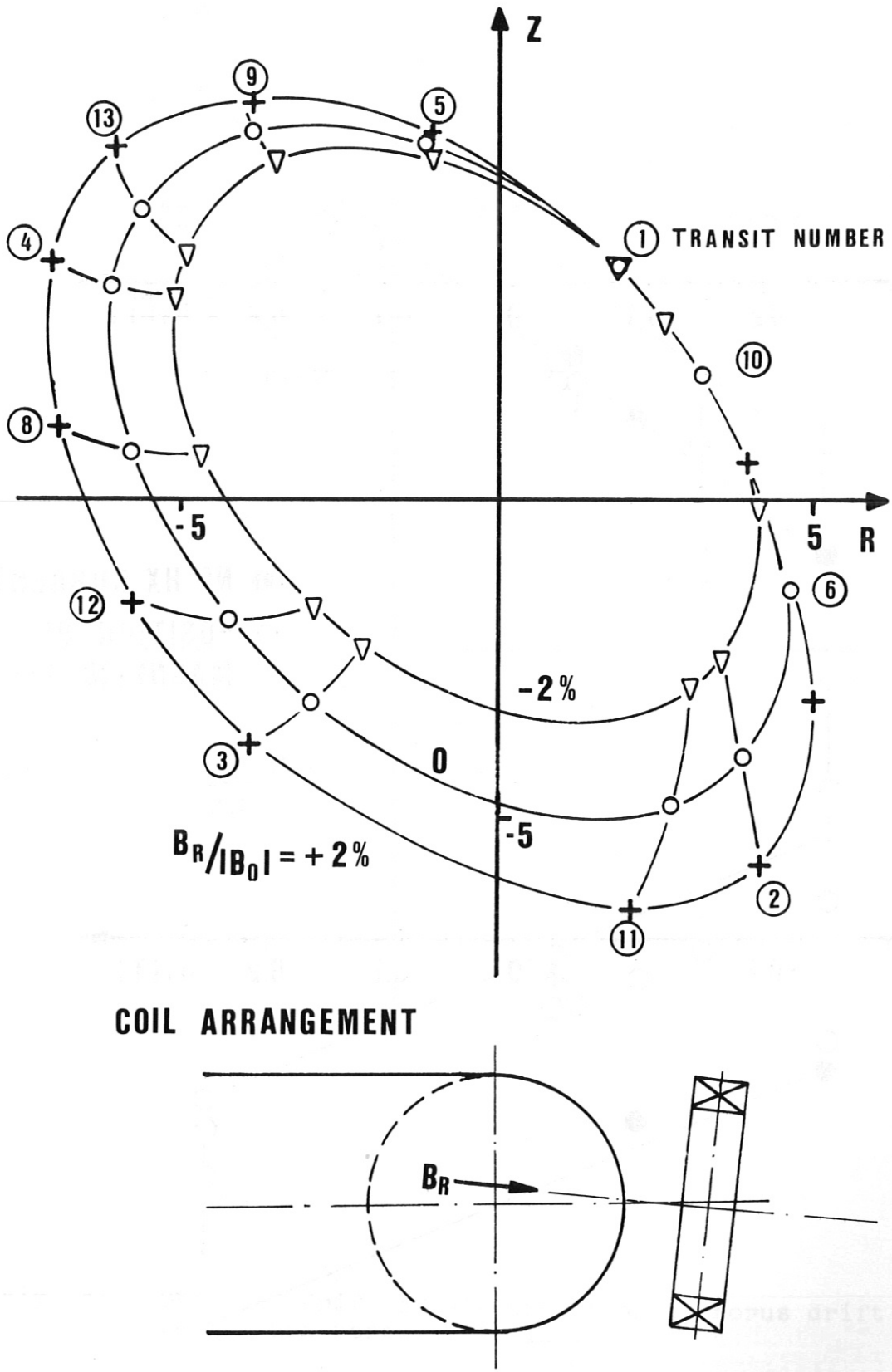

Fig. 10: Experimental magnetic surfaces obtained by local field of coil arrangement (shown in the lower half of the figure) superimposed to the standard case configuration.

MAGNETIC SURFACES AT $\iota \approx 1/4$

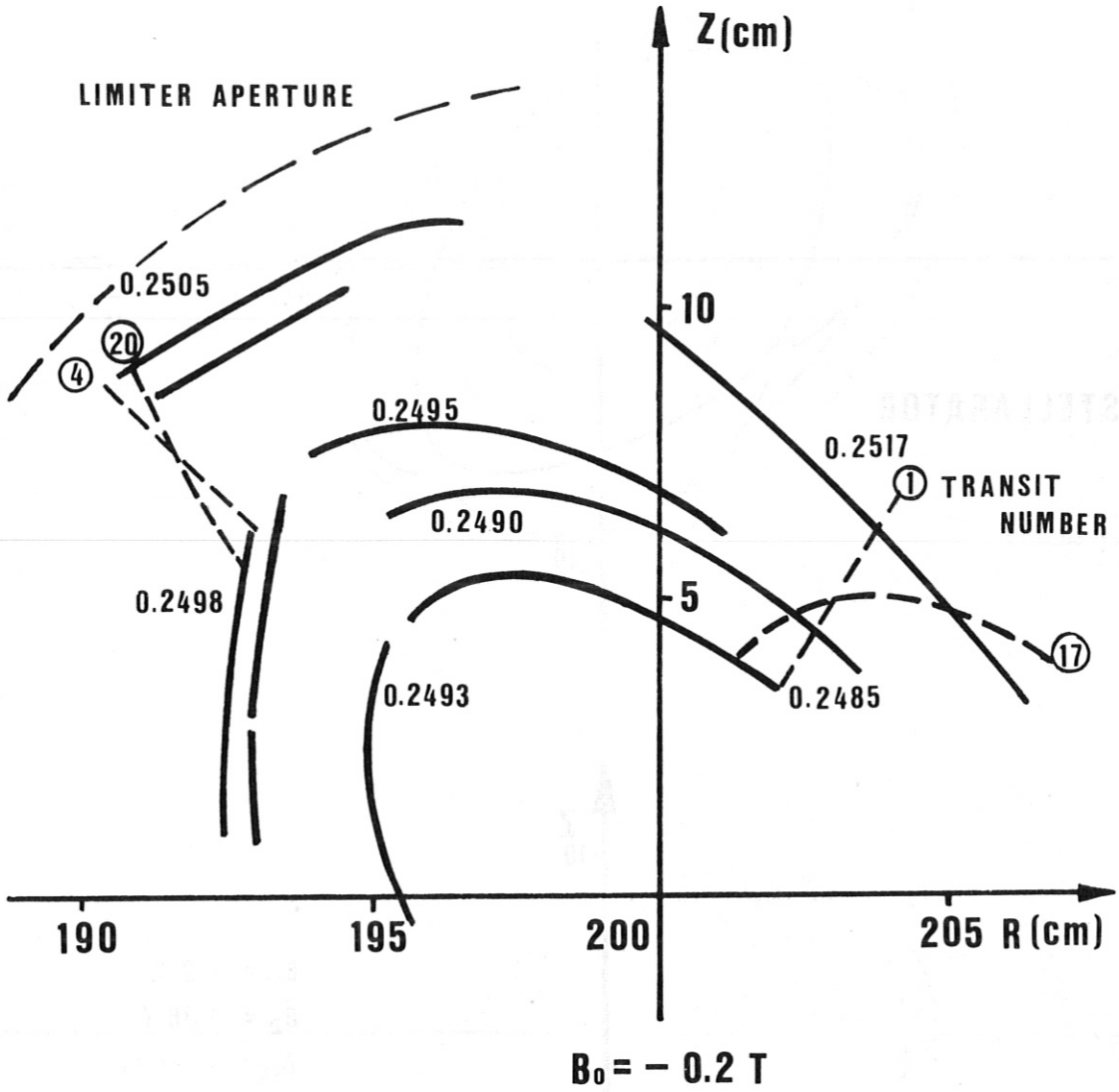

Fig. 11: Experimental magnetic surfaces at $\iota \approx 1/4$.

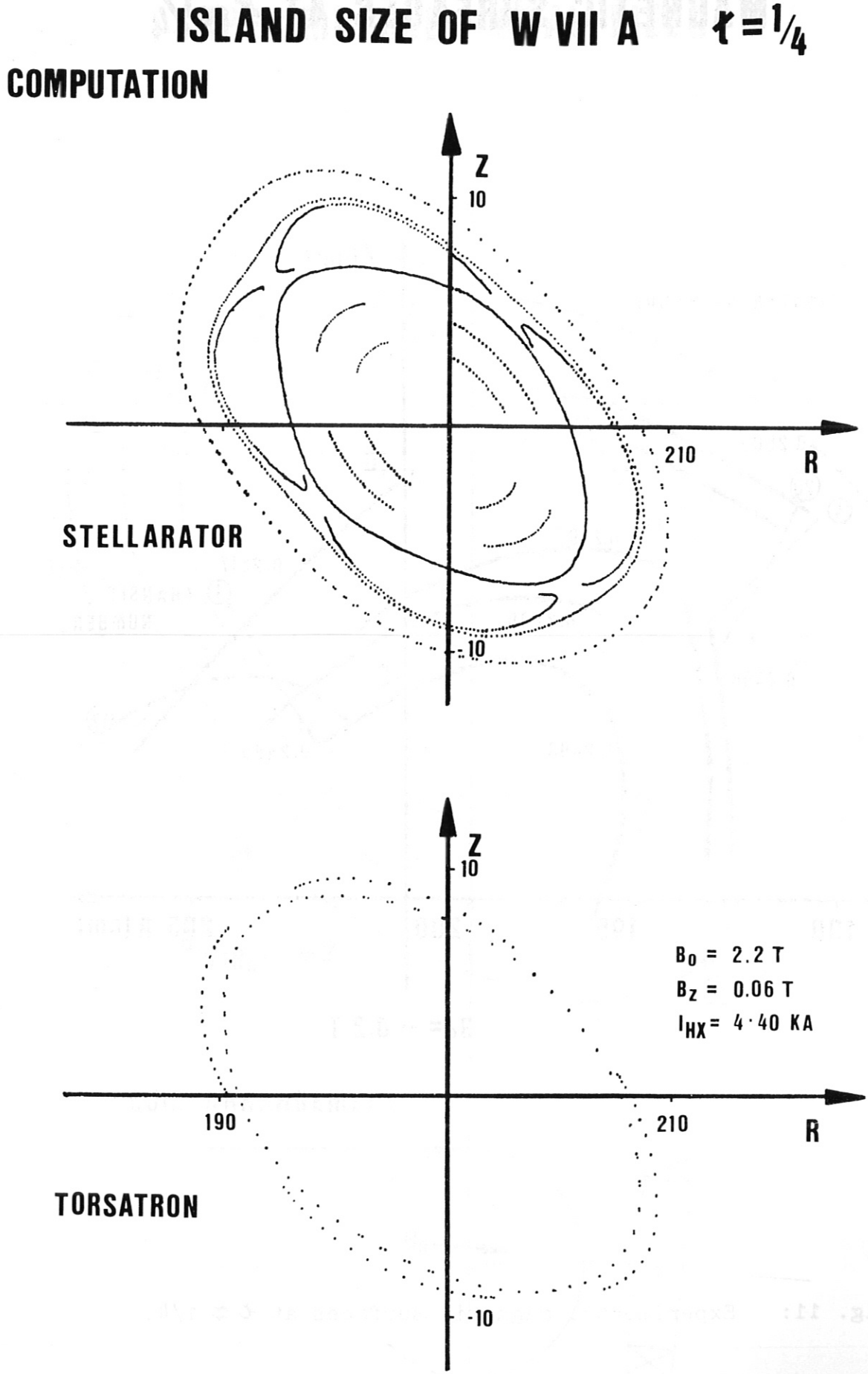

Fig. 12: Computed magnetic islands at ι = 1/4 due to certain construction elements of the W VII A helix, for stellarator configuration (upper half) and torsatron configuration (lower half) of W VII A.